

Molecular tracers of planet formation in the atmospheres of hot Jupiters

Richard Hobbs,¹★ Oliver Shorttle,^{1,2} And Nikku Madhusudhan¹

¹*Institute of Astronomy, University of Cambridge, Cambridge, CB3 0HA, UK*

²*Cambridge Earth Sciences, University of Cambridge, Cambridge CB2 3EQ, UK*

Accepted XXX. Received YYY; in original form ZZZ

ABSTRACT

The atmospheric chemical composition of a hot Jupiter can lead to insights into where in its natal protoplanetary disk it formed and its subsequent migration pathway. We use a 1-D chemical kinetics code to compute a suite of models across a range of elemental abundances to investigate the resultant abundances of key molecules in hot Jupiter atmospheres. Our parameter sweep spans metallicities between 0.1x and 10x solar values for the C/H, O/H and N/H ratios, and equilibrium temperatures of 1000K and 2000K. We link this parameter sweep to the formation and migration models from previous works to predict connections between the atmospheric molecular abundances and formation pathways, for the molecules H₂O, CO, CH₄, CO₂, HCN and NH₃. We investigate atmospheric H₂O abundances in eight hot Jupiters reported in the literature. All eight planets fall within our predicted ranges for various formation models, however six of them are degenerate between multiple models and, hence, require additional molecular detections for constraining their formation histories. The other two planets, HD 189733 b and HD 209458 b, have water abundances that fall within ranges expected from planets that formed beyond the CO₂ snowline. Finally, we investigate the detections of H₂O, CO, CH₄, CO₂, HCN and NH₃ in the atmosphere of HD 209458 b and find that, within the framework of our model, the abundances of these molecules best match with a planet that formed between the CO₂ and CO snowlines and then underwent disk-free migration to reach its current location.

Key words: planets and satellites: gaseous planets – planets and satellites: atmospheres – planets and satellites: composition – planets and satellites: formation – planets and satellites: individual (HD 209458b)

1 INTRODUCTION

The location where a Jupiter-like planet forms around a star can leave traces upon the chemical composition of its atmosphere. Planets are formed out of the dust and gas surrounding their host star. Therefore, any variations in the composition of the gas or dust in the protoplanetary disk that depend on the distance from the star should still be evident in the planet itself, depending on the ratio of dust to gas it is formed from (e.g., Öberg et al. 2011; Helling et al. 2014; Madhusudhan et al. 2014b; Cridland et al. 2016; Madhusudhan et al. 2016; Mordasini et al. 2016; Venturini et al. 2016; Booth et al. 2017; Eistrup et al. 2018; Pudritz et al. 2018; Madhusudhan 2019; Khorshid et al. 2021).

At greater radial distances in the disk, various volatile species pass their snowlines, where they transition from the gas phase into being frozen as ice. In particular, oxygen rich species such as H₂O and CO₂ have their snowlines at higher temperatures (and therefore

closer to the star) than CO: The water snowline in the disk mid-plane is typically at ~170 K, the CO₂ is at ~80 K and the CO snowline is at ~30 K (Martín-Doménech et al. 2014). Thus, the solids throughout most of the disk have sub-solar C/O ratios, and the gas has a super-solar C/O ratio. Furthermore, the C/H and O/H ratios of the gas are sub-solar outside the snowlines of the corresponding molecules. In the same way, the N/H ratio in the gas becomes sub-solar once NH₃ freezes out at ~100 K (Martín-Doménech et al. 2014).

There are two routes through which a gas giant is expected to form; core accretion closer to the star (Pollack et al. 1996; Lissauer & Stevenson 2007), and gravitational instability further from the star (Boss 2000; Gammie 2001; Boley 2009; Boley & Durisen 2010; Forgan & Rice 2011). In the gravitational instability scenario the planet forms early and quickly, accreting dust and gas almost simultaneously. As such, such planets are typically expected to have a similar bulk composition to that of the disk as a whole, and therefore similar to the stellar metallicity (Boss 1997; Helled & Bodenheimer 2010). However, more recent work has shown that it is possible for planets formed via gravitational instability to have

★ E-mail: rh567@cam.ac.uk

enriched or depleted metallicities based upon the size of the solids being accreted; if most solids are between 0.1m and 100m the resulting planet can become enriched, while if most solids are above 1km the planet may end up depleted (Helled et al. 2014). For the core accretion scenario a planet’s resulting atmospheric metallicity is a more complicated function of planet location, being dependent on the solid to gas partitioning of elements. Most models of core accretion require several million years to form a rocky core and accrete a gaseous envelope (e.g., Pollack et al. 1996; Lissauer & Stevenson 2007; Kobayashi et al. 2011). The composition of the accreted gas is dependent upon the location of the forming planet within the disk. However, enrichment of the atmosphere by solids can also occur during atmospheric accretion, resulting in a variable overall composition (Pollack et al. 1996).

However, there are challenges to linking gas giant atmospheric composition directly to formation location. The presence of hot Jupiters suggests that giant planets can migrate through their system. This is because gaseous giant planets are not expected to form on such short period orbits (e.g., Mayor & Queloz 1995; Wu & Murray 2003; Papaloizou et al. 2007; Wu & Lithwick 2011). The accretion of solids (in the form of planetesimals or core erosion) onto the gas giant can result in a significantly different atmospheric composition, especially if solid accretion occurs during migration. Accretion of solids typically results in planetary compositions that are solar or super-solar in O/H and C/H but sub-solar in C/O ratio, since the solids within the CO snow line are oxygen rich (e.g., Öberg et al. 2011; Madhusudhan et al. 2014b; Venturini et al. 2016; Mordasini et al. 2016). On the other hand, formation of giant planets beyond the H₂O, CO₂ or CO snowlines without significant solid accretion followed by disk free migration can result in low atmospheric metallicities and high C/O ratios (e.g. Madhusudhan et al. 2014b). Additionally, radial drift of icy grains from the outer disk can supply volatiles to the inner disk (Booth et al. 2017). This results in the enrichment of volatiles at the snowlines of up to 10× C/H or O/H. This allows gas giants to become metal rich by directly accreting metal-rich gas, and opens the possibility of planets with super-solar C/H and super-solar C/O. Recently, studies have also investigated how N/H ratios may vary in a planet’s atmosphere based upon where the planet forms (Bosman et al. 2019; Öberg & Wordsworth 2019; Turrini et al. 2021). This additional parameter may help to break some of the degeneracy when examining the composition of giant planets, refining the estimates of where a particular planet may have formed.

Some studies have examined how the molecular composition of a hot Jupiter may vary based on its elemental abundances (Madhusudhan 2012; Moses et al. 2013; Tsai et al. 2017), and others have studied how the elemental abundances may change based on where the hot Jupiter formed and how it migrated (e.g. Madhusudhan et al. 2014b; Mordasini et al. 2016; Cridland et al. 2020). However, very few have tried to link these two regimes such that it becomes possible to predict where a hot Jupiter formed based upon its molecular composition. Those that have attempted to do so typically use local thermochemical equilibrium models (Mordasini et al. 2016). However, purely chemical equilibrium models are not adequate to fully represent the atmospheric chemistry of hot Jupiters.

When considering nitrogen bearing species, thermochemical models of Hot Jupiters with atmospheric temperatures above 700 K predict N₂ to be the dominant nitrogen bearing molecule at around 1 bar (e.g., Moses et al. 2011; Venot et al. 2012). N₂ is not detectable by spectral observations, which in principle makes determining the N/H ratio of hot Jupiter atmospheres challenging. However, there have been potential detections of the nitrogen bearing molecules

NH₃ and HCN in the atmosphere of HD209458b, a planet whose temperature is far above 700 K (Giacobbe et al. 2021). This would only be possible if disequilibrium chemical effects, such as diffusion and photochemistry, were impacting the composition of the planet’s atmosphere. As such, in this work, we compute a full suite of disequilibrium chemical models over the range of C/H, O/H and N/H ratios expected from planet formation models. In doing so we aim to more accurately link the observed molecular abundances of hot Jupiter observations to the planet’s elemental composition, and thus to the planet’s formation and migration history.

In Section 2.1 we provide details of the chemical kinetics code we are using to create our models, as well as the atmospheric parameters of the hot Jupiters we are modelling. We present the results of these models in Section 3. In Section 4 we discuss the results of our models, and compare them with different formation scenarios from previous works. We compare our models to observed molecular abundances in some hot Jupiters in Section 5. We discuss our findings and review our work in Section 6.

2 METHODS

2.1 The Atmospheric Model

To calculate the abundance of HCNO species throughout the atmospheres of hot Jupiters, we choose to use a chemical kinetics code that can model the effects of disequilibrium chemistry in these atmospheres. We previously developed a disequilibrium chemical kinetics code, LEVI, to model hot Jupiter atmospheres. The full development, testing and benchmarking of this code can be found in Hobbs et al. (2019). A summary of the salient points from this previous work, and a description of changes made to the model for this work will be provided in this section.

The code, LEVI, in this work is being used to model the atmospheric chemistry of Jupiter like planets. It does so by calculating the interactions between chemical species, the effects of vertical mixing due to eddy-diffusion, molecular diffusion and thermal diffusion, and photo-chemical dissociation due to an incoming UV flux. It uses input parameters such as the desired equilibrium temperature of the planet and the planet’s radius, profiles for the UV stellar spectrum, the pressure-temperature (P-T) profile of the atmosphere, and the eddy-diffusion (K_{zz}) profile. It uses the assumptions of hydro-static equilibrium, the atmosphere being an ideal gas, and that the atmosphere is small compared to the planet, such that gravity is constant throughout the atmospheric range being modelled.

In this work, as in Hobbs et al. (2019), we will limit our network to exploring the chemistry of H, He, C, N, O species. It is possible that species containing other elements could affect the results produced. There are some cases in which sulfur chemistry (Zahnle et al. 2016; Hobbs et al. 2021) can impact the results of this paper. However, the inclusion of these sulfur species goes beyond the scope of this work.

As is typical for codes of this type, we solve the coupled one-dimensional continuity equation:

$$\frac{\partial n_i}{\partial t} = \mathcal{P}_i - \mathcal{L}_i - \frac{\partial \Phi_i}{\partial z}, \quad (1)$$

where n_i (m⁻³) is the number density of species i , with $i = 1, \dots, N$, with N being the total number of species. \mathcal{P}_i (m⁻³ s⁻¹) and \mathcal{L}_i (m⁻³ s⁻¹) are the production and loss rates of the species i . ∂t (s) and ∂z (m) are the infinitesimal time step and altitude step

respectively. Φ_i ($\text{m}^{-2} \text{s}^{-1}$) is the upward vertical flux of the species, given by,

$$\Phi_i = -(K_{zz} + D_i)n_i \frac{\partial X_i}{\partial z} + D_i n_i \left(\frac{1}{H_0} - \frac{1}{H} - \frac{\alpha_{T,i}}{T} \frac{dT}{dz} \right), \quad (2)$$

where X_i is the mixing ratio of molecule i , and n_i (m^{-3}) is the total number density of molecules such that $n_i = X_i n_t$. The eddy-diffusion coefficient, K_{zz} ($\text{m}^2 \text{s}^{-1}$), approximates the rate of vertical transport and D_i ($\text{m}^2 \text{s}^{-1}$) is the molecular diffusion coefficient of species i . H_0 (m) is the mean scale height of the atmosphere, H (m) is the molecular scale height, T (K) is the temperature, and $\alpha_{T,i}$ is the thermal diffusion factor. For the full explanation of how we determine each of these parameters, and solved the equations, see [Hobbs et al. \(2019\)](#).

Unlike in the previous work, we no longer use precalculated K_{zz} profiles, instead we calculate the profile iteratively and self-consistently using the equations described in [Zhang & Showman \(2017\)](#) and [Komacek et al. \(2019\)](#):

$$K_{zz} \sim \frac{W^2}{\tau_{\text{chem}}^{-1} + \frac{W}{H}}, \quad (3)$$

where $H = RT/g$ is the scale height of the atmosphere, with R being the gas constant, T being the temperature at the pressure being calculated and g being the gravitational acceleration of the planet. τ_{chem} is the timescale of chemical interactions, and is equal to:

$$\tau_{\text{chem}} = \frac{[X]}{d[X]/dt}, \quad (4)$$

where $[X]$ is the abundance of some molecule X , and W is the vertical wind speed, where $\frac{W}{H} \sim \frac{U}{a}$. Here, a is the radius of the planet, and U is the characteristic horizontal wind-speed, defined as

$$U \sim \frac{2\gamma U_{\text{eq}}}{\alpha + \sqrt{\alpha^2 + 4\gamma^2}}, \quad (5)$$

where U_{eq} is the speed of the maximum cyclostrophic wind, defined as

$$U_{\text{eq}} = \frac{a}{\tau_{\text{adv,eq}}}, \quad (6)$$

and the dimensionless parameters α and γ are defined as

$$\alpha = 1 + \frac{\Omega \tau_{\text{wave}}^2}{\tau_{\text{rad}} \Delta \ln p}, \quad (7)$$

$$\gamma = \frac{\tau_{\text{wave}}^2}{\tau_{\text{rad}} \tau_{\text{adv,eq}} \Delta \ln p}. \quad (8)$$

Ω is the planet's rotation rate, set equal to the orbital period in this work since we assume hot Jupiters are always tidally locked. $\Delta \ln p$ is the pressure difference between the pressure of interest and the deep atmosphere, where the day and night temperatures are the same. The timescales in the above equations are: The Kelvin wave propagation time across a hemisphere;

$$\tau_{\text{wave}} = a/NH, \quad (9)$$

where N is the Brunt-Väisälä frequency, the radiative timescale;

$$\tau_{\text{rad}} = \frac{p c_p}{4 g \sigma T^3}, \quad (10)$$

where c_p is the specific heat capacity of the atmosphere, and σ is

the Stefan-Boltzmann constant. Lastly, the advective timescale that a cyclostrophic wind induced by the day-night temperature difference in radiative equilibrium would have is;

$$\tau_{\text{adv,eq}} = a \sqrt{\frac{2}{R k_b T_{\text{eq}} \Delta \ln p}}, \quad (11)$$

where k_b is the Boltzmann constant and T_{eq} is the equilibrium temperature of the planet.

We also use a variable parametrisation for the P-T profile of the atmosphere using the equations described in [Guillot \(2010\)](#). The temperature of the atmosphere is parametised as;

$$T^4 = \frac{3}{4} T_{\text{int}}^4 \left(\frac{2}{3} + \tau \right) + \frac{3}{4} T_{\text{irr}}^4 f \left(\frac{2}{3} + \frac{\mu_*}{\gamma} + \left(\frac{\gamma}{3\mu_*} - \frac{\mu_*}{\gamma} \right) \exp\left(-\frac{\gamma \tau}{\mu_*}\right) \right). \quad (12)$$

Here, $\mu_* = \cos \theta_* = 1/\sqrt{3}$, where θ_* is the incidence angle for stellar radiation, $\gamma = \kappa_v/\kappa_{\text{th}}$ is the ratio between the mean visual (κ_v) and thermal (κ_{th}) opacities, and τ is the optical depth. We chose the values for the visual and thermal opacities to be $4 \times 10^{-3} \text{ cm}^2 \text{ g}^{-1}$ and $10^{-2} \text{ cm}^2 \text{ g}^{-1}$ respectively, approximately the values for HD 209458b ([Guillot 2010](#)). $f = 1/2$ is a flux factor for isotropic radiation averaged over the day-side of the planet. The interior temperature is set to be $T_{\text{int}} = 300 \text{ K}$ and the irradiation temperature is $T_{\text{irr}} = \sqrt{2} T_{\text{eq}}$, where T_{eq} is the equilibrium temperature of the planet. For T_{eq} we assume the planet has an albedo of 0 and efficient energy redistribution.

We use the values for solar metallicity from [Asplund et al. \(2009\)](#). This gives an elemental ratio, as a fraction of the total number of molecules, of: $X_{\text{H}_2} = 0.5 \times X_{\text{H}} = 0.8535$, $X_{\text{He}} = 0.145$, $X_{\text{C}} = 4.584 \times 10^{-4}$, $X_{\text{O}} = 8.359 \times 10^{-4}$, $X_{\text{N}} = 1.154 \times 10^{-4}$. In our models, we independently alter the metallicity between 0.1x and 10x these solar values for each of C, O, N. He is kept constant, and H_2 is altered such that X_{H_2} , X_{He} , X_{C} , X_{O} and X_{N} sum to unity.

The equilibrium temperatures of the modelled hot Jupiters range across five temperatures between 1000 K and 2000 K, although we only show the two extremes in this work. To produce a suite of models over the full range of bulk compositions, we ran our model for each point in a $9 \times 9 \times 9$ grid in the C/H, O/H and N/H parameter space, for each planetary equilibrium temperature being investigated. This produced a total of 729 models per modelled planet, with data points for X/H equally spaced in logspace between 0.1x and 10x the solar values for X/H.

It is worth noting that due to our prescription for K_{zz} , the different equilibrium temperatures of our hot Jupiter models will result in different K_{zz} values. While this masks the exclusive effect of temperature as a variable in setting the chemistry of hot Jupiter atmospheres, our primary aim is to model realistic variations in hot Jupiter atmospheric chemistry due to compositional differences. Therefore, a sweep of orbital radius (and therefore temperature and K_{zz}), explores the range of hot Jupiter atmosphere chemistry for a given composition.

2.2 Planet composition models

In this section we discuss how different formation and migration mechanisms may lead to different metallicities in the atmosphere of a hot Jupiter. Throughout this work we use metallicity to refer to the full suite of C/H, O/H and N/H ratios, and we use the convention that X/H refers to the absolute value, while [X/H] refers to a value

normalised to the solar abundances. We use the values for solar from [Asplund et al. \(2009\)](#). The following formation and migration pathways came from three different works; [Madhusudhan et al. \(2014b\)](#), [Booth et al. \(2017\)](#) and [Turrini et al. \(2021\)](#).

The work of [Madhusudhan et al. \(2014b\)](#) does not consider nitrogen composition, however, they do consider the widest range of formation scenarios of the studies we draw from. They model hot Jupiters that formed via core accretion and then migrated via both in-disk and disk-free migration, as well as hot Jupiters that formed via gravitational instability before migrating disk-free. This produces a wide range of potential C/O ratios for a hot Jupiter, based upon its history.

[Madhusudhan et al. \(2014b\)](#) found that hot Jupiters formed by core accretion between 2 AU and 20 AU before undergoing disk migration had $1 < [\text{O}/\text{H}] < 10$, and $1 < [\text{C}/\text{H}] < 5$, with a C/O ratio that was always sub-solar. Hot Jupiters that formed by core accretion but then underwent disk-free migration fall into two regimes. Those that formed closer in have slightly super-solar C/H and O/H, up to $[\text{C}/\text{H}] = 2$ and $[\text{O}/\text{H}] = 4$, but still sub-solar C/O, while those that formed further away, beyond the CO_2 snowline, had sub-solar C/H and O/H, down to $[\text{C}/\text{H}] = 0.6$ and $[\text{O}/\text{H}] = 0.4$, but a super-solar C/O ratio. Lastly, planets that formed beyond the CO_2 snowline but within the CO snowline by gravitational instability and then migrated inwards also tend to have either super-solar metallicity but a sub-solar C/O ratio or sub-solar metallicity with a super-solar C/O ratio. However, if they formed beyond the CO snowline, beyond ~ 100 AU, they can be any metallicity within our parameter space, but at a solar C/O ratio.

The work of [Booth et al. \(2017\)](#) also does not consider nitrogen in their models. However, their models of chemical enrichment by pebble drift result in compositions in regions of the parameter space that were forbidden by previous works. Through the accretion of metal rich gas the composition of a gas giant could end up with a $[\text{C}/\text{H}]$ ratio up to 5, and a C/O ratio between solar (0.55) and 1. For Jupiter mass planets forming within the CO_2 snowline, [Booth et al. \(2017\)](#) tend to find metallicities of $[\text{O}/\text{H}] = 2$ and between $2 < [\text{C}/\text{H}] < 3$, thus producing super-solar C/O ratios in these high metallicity planets. For planets forming beyond the CO_2 snowline, most formation locations result in a C/O ratio of 1, along the entire parameter space of metallicities.

[Turrini et al. \(2021\)](#) do not consider as wide a range of migration routes as the previous works we have compared to, but they do include the nitrogen in their models as a possible way of breaking the degeneracy arising from consideration of only the C/O ratio. They consider 6 different formation locations for a hot Jupiter that forms via core accretion and subsequently migrates through the disk to an orbital radius of 0.04 AU, accreting solids along the way. How these formation locations relate to the atmospheric C/H, O/H and N/H ratios compared to their solar values is summarised in Table 1. While we acknowledge that our planetary models orbit at slightly wider radii (between 0.08 AU and 0.3 AU) compared to the 0.04 AU in the work of [Turrini et al. \(2021\)](#), we assume that any change in the atmospheric composition due to these small differences in migration distance will be sufficiently small to ignore.

A summary of the different metallicities expected from these formation models can be seen in Figure 1.

3 MODEL RESULTS

In this section we present the results of our suite of chemical models. We compute models over a grid of C/H, O/H and N/H ratios

a (AU)	[C/H]	[O/H]	[N/H]
5	0.93	1.06	1.02
12	1.33	1.28	1.09
19	1.77	1.85	1.35
50	3.23	3.70	1.89
100	4.67	5.19	2.43
130	7.33	8.33	3.65

Table 1. A summary of the expected bulk compositions of a hot Jupiter from [Turrini et al. \(2021\)](#). The planet starts migrating from 6 different formation locations, accreting solids as it travels inwards until its final position at 0.04 AU.

for two hot Jupiters. We discuss example hot Jupiters at two limiting equilibrium temperatures; 1000 K and 2000 K. These planets correspond to an orbital radius of 0.3 AU and 0.08 AU around a Sun-like star respectively, assuming an albedo of 0 and efficient energy redistribution. We show the resultant P-T profiles for these planets in Figure 2 and the K_{zz} profiles in Figure 3.

Results of the parameter sweep are shown in Figures 4 - 9, presented below. In these figures, we show the C/O ratios of 0.25, 0.54 (solar) and 1 as lines on the figures to assist in determining the abundances at these values. Additionally, we split each figure into three regimes; abundances above 10^{-6} which should be detectable, abundances between 10^{-6} and 10^{-10} which we may one day be able to detect and abundances below 10^{-10} which we never expect to be detectable ([Greene et al. \(2016\)](#)). All these results are shown for a pressure of 10^{-3} bar, the pressure at which observations of the molecules we model are sensitive to in hot Jupiter atmospheres ([Madhusudhan \(2019\)](#)).

3.1 H_2O abundance

In Figure 4 we show how the abundance of water varies over our chosen parameter space. Water's abundance is primarily determined by O/H, however for C/O ratio values greater than 1, a decrease in the abundance of water can be seen ([Madhusudhan 2012](#); [Moses et al. 2013](#)). This is because water does have a weak dependence on the C/H ratio; as the C/O ratio approaches 1, the fraction of O in CO becomes increasingly significant, leaving less O to form H_2O . While $\text{C/O} < 1$, we see a range in H_2O abundances between 10^{-5} at $[\text{O}/\text{H}] = 0.1$ and 10^{-2} at $[\text{O}/\text{H}] = 10$ for both temperature models. For C/O ratios greater than 1, the H_2O abundance on the 1000 K hot Jupiter slowly decreases down to 10^{-6} as the C/O ratio increases, while on the 2000 K hot Jupiter, the H_2O drops by several orders of magnitude immediately.

For planets with a C/O ratio close to 1, H_2O is a good measure of the C/O ratio in our two hot Jupiter models. This is because the H_2O becomes increasingly dependent on the C/O ratio once the ratio approaches or exceeds 1. For C/O ratios that exceed 1 in our 2000K model, the abundance of H_2O would drop below detectable limits, and would not contribute significantly to the measured C/O ratio. However, water can still act as a diagnostic for the C/O ratio, even for C/O ratios great than 1, since the lack of water is itself a diagnostic. At C/O ratios less than 0.25, the H_2O abundance tends to depend only on the O/H ratio, becoming a worse measure of the C/O ratio. As expected for H_2O , it is independent of the N/H ratio. There are no N-based species that contain O that are of sufficient abundance to impact the sequestration of O in H_2O . Thus, H_2O has no use in determining the N/H ratio.

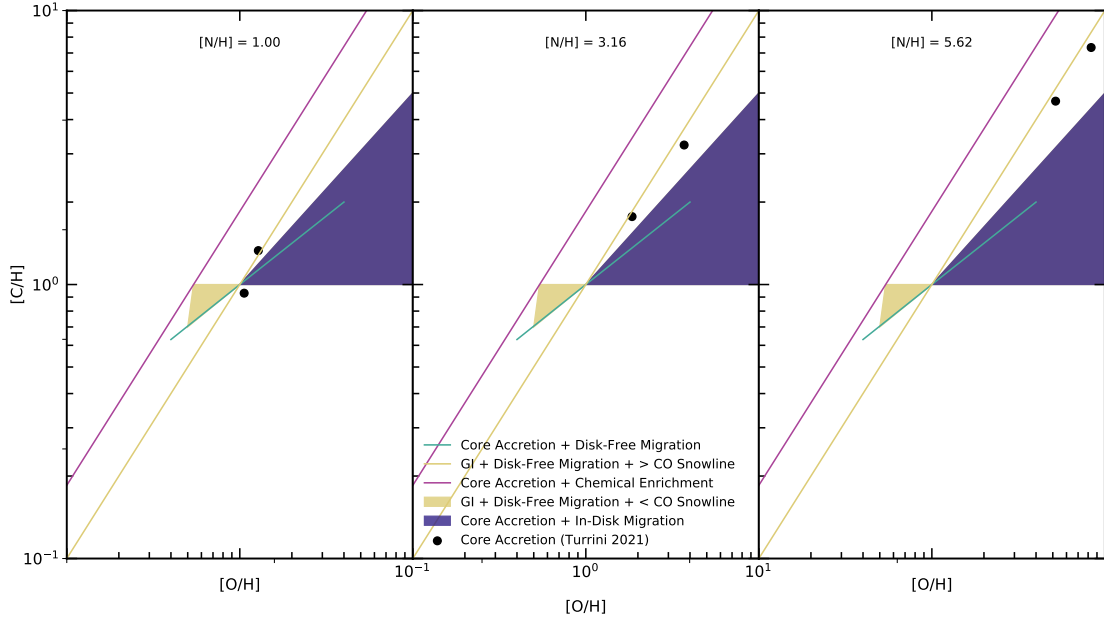


Figure 1. The different ranges of metallicities expected from several formation models. The indigo, cyan and yellow lines cover the core accretion and gravitational instability models from [Madhusudhan et al. \(2014b\)](#), the purple lines covers the pebble accretion and enrichment models from [Booth et al. \(2017\)](#), and the black dots are the metallicities expected from the six formation locations for core accretion in [Turrini et al. \(2021\)](#). Gravitational instability from within the CO snowline also covers the entire metallicity range of Core Accretion with in-disk migration, but can't be easily seen due to overlap.

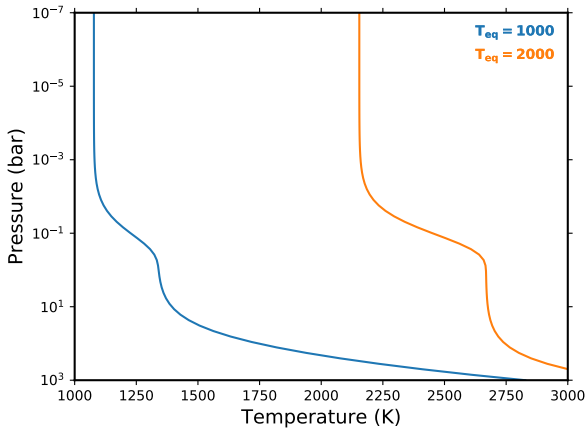


Figure 2. The P-T profiles being used in this work. Both were created using the expression presented in Section 2.1, with an equilibrium temperature of 1000 K or 2000 K.

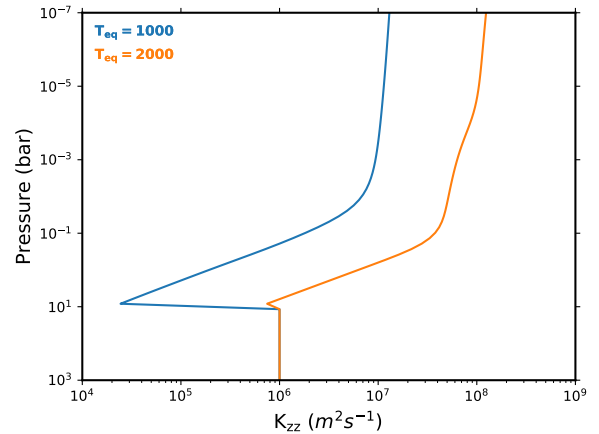


Figure 3. The K_{zz} profiles being used in this work. Both were created using the expression presented in Section 2.1, with an equilibrium temperature of 1000 K or 2000 K.

3.2 CO abundance

Figure 5 shows how the abundance of CO varies across the composition parameter space. CO is directly dependent upon both the O/H and C/H ratios. However, the way it is dependent can be quite useful for determining planetary composition. For a C/O ratio less than 1, the CO abundance is near independent of the O/H ratio, while for a C/O ratio greater than 1, the CO abundance is near independent of the C/H ratio. This is because for $C/O < 1$, CO is the primary carbon carrier, and as long as there is more oxygen than carbon, increasing

the amount of oxygen does not assist in creating more CO. This relationship is reversed for ratios of $C/O > 1$. Since there are very few formation models that result in a $C/O > 1$, we can see that CO provides a good measure of the C/H ratio, especially considering that it is predicted to be one of the most abundant species in hot Jupiter atmospheres. In our modelled atmospheres, we find that the abundance of CO varies between 10^{-5} for $[O/H] = 0.1$ and $[C/H] = 0.1$, and 10^{-2} for $[O/H] = 10$ and $[C/H] = 10$. Once again, we see little effect of the N/H ratio on the abundance of CO. While molecules like HCN could theoretically take more of the available

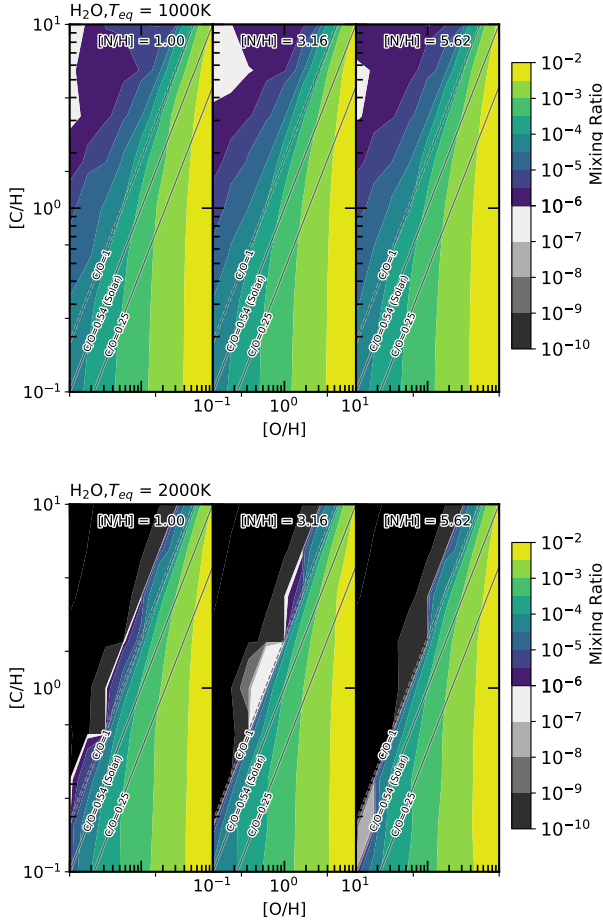


Figure 4. The abundance of H_2O for two hot Jupiters, one with a 1000 K equilibrium temperature (top) and one with a 2000 K equilibrium temperature (bottom). The variation in abundance of H_2O is shown against the atmospheric C/H and O/H ratios normalised to solar values. The C/O ratios of 0.25, 0.54 (solar) and 1 are shown on each plot to assist visualisation. Additionally, we consider three atmospheric N/H ratios normalised to solar; 1, 3.2 and 5.6. These are shown from left to right on the figures above.

carbon as the N/H ratio increases, we find that even with $[\text{N}/\text{H}] = 10$, the HCN abundance is still a small fraction of the CO abundance and thus doesn't diminish the atmospheric CO reservoir in any significant way.

3.3 CH_4 abundance

The variation in the methane abundance across our parameter space is shown in Figure 6. We find CH_4 has a positive dependence upon the C/H ratio and a negative dependence upon the O/H ratio for the two hot Jupiters we model. This is due to CO sequestering a greater fraction of the carbon as the amount of available O in the atmosphere increases. Unlike H_2O and CO, methane's abundance also has a strong temperature dependence. At 1000 K, CH_4 has a maximal abundance of 10^{-2} in the high C/H, low O/H regime, with a minimal abundance of 10^{-8} in the low C/H, high O/H regime. By comparison, at 2000 K, the maximum and minimum abundance of methane is 10^{-6} and 10^{-16} respectively. Methane's abundance is approximately unchanging along lines of constant C/O ratio, making it an excellent check to confirm the values of the C/O first expected

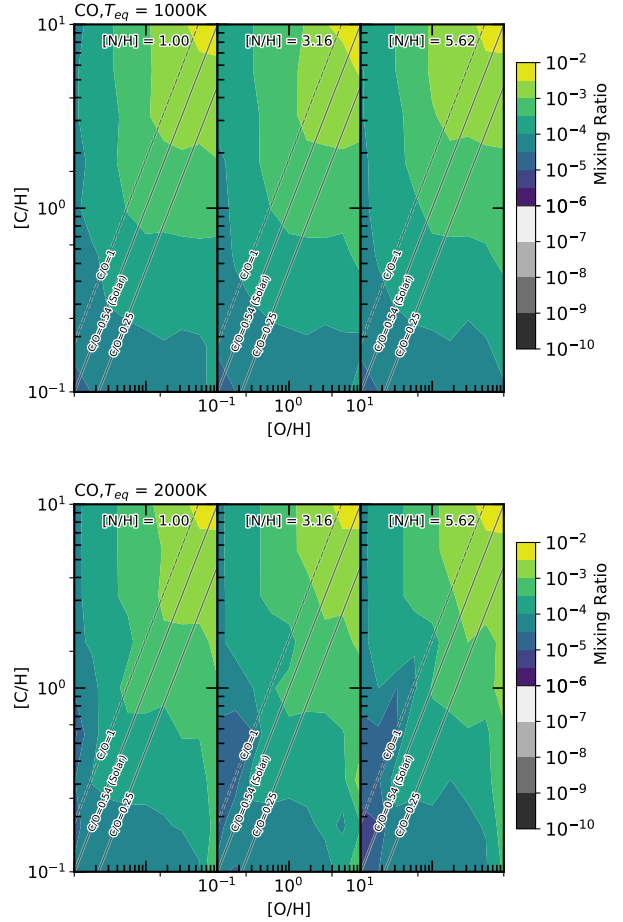


Figure 5. The abundance of CO for two hot Jupiters, one with a 1000 K equilibrium temperature (top) and one with a 2000 K equilibrium temperature (bottom). The variation in abundance of CO is shown against the atmospheric C/H and O/H ratios normalised to solar values. The C/O ratios of 0.25, 0.54 (solar) and 1 are shown on each plot to assist visualisation. Additionally, we consider three atmospheric N/H ratios normalised to solar; 1, 3.2 and 5.6. These are shown from left to right on the figures above.

by examining CO and H_2O . However, it will likely be impossible to detect CH_4 on the hotter hot Jupiters; in our 2000 K model, for a $\text{C}/\text{O} < 1$, methane's abundance is typically below 10^{-9} . This is far below the estimates we have for the detectable limits of molecules. The strong dependence of the CH_4 abundance on temperature does make it a good proxy for the temperature, but a poor tool for examining the metallicity of the very hot Jupiters.

3.4 CO_2 abundance

We show the range of CO_2 abundances in Figure 7. We find that CO_2 is very strongly dependent on the O/H ratio, but only weakly dependent on the C/H ratio in our models. However, there is a significant decrease in CO_2 abundance when the C/O ratio crosses from less than 1 to greater than 1. This is because, for $\text{C}/\text{O} > 1$, the majority of the oxygen is sequestered in the form of CO, leaving little available for other oxygen bearing species. The range of CO_2 abundances in both temperature cases are similar for C/O ratios less than 1, ranging between 10^{-9} and 10^{-4} . Though for $\text{C}/\text{O} > 1$, CO_2 follows a similar pattern to H_2O , for $T_{\text{eq}} = 2000$ K there is a rapid

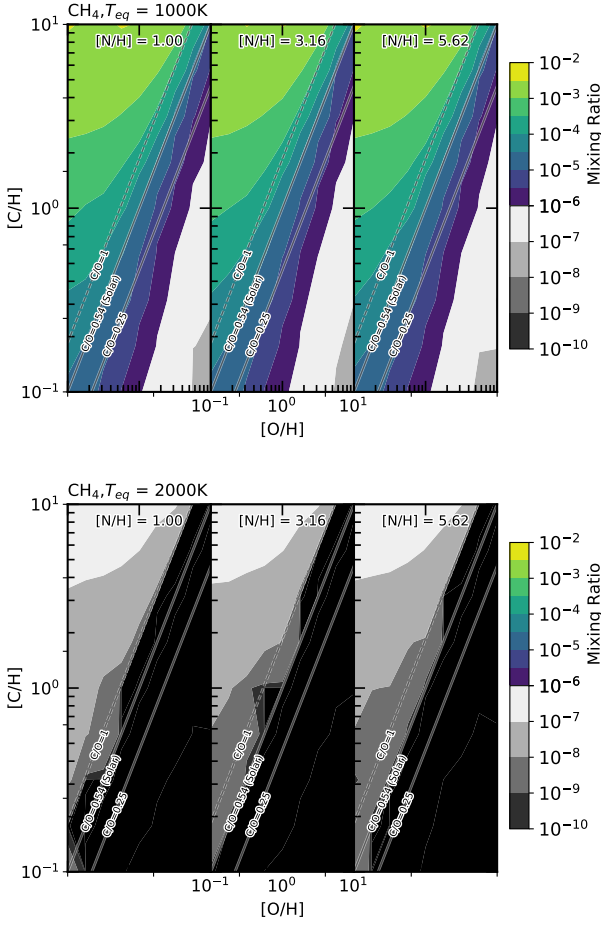


Figure 6. The abundance of CH_4 for two hot Jupiters, one with a 1000 K equilibrium temperature (top) and one with a 2000 K equilibrium temperature (bottom). The variation in abundance of CH_4 is shown against the atmospheric C/H and O/H ratios normalised to solar values. The C/O ratios of 0.25, 0.54 (solar) and 1 are shown on each plot to assist visualisation. Additionally, we consider three atmospheric N/H ratios normalised to solar; 1, 3.2 and 5.6. These are shown from left to right on the figures above.

decline in abundance as the C/O ratio increases, while for $T_{eq} = 1000$ K the decline is much slower. CO_2 is a poor diagnostic tool by itself, with a large range of both C/H and O/H ratios corresponding to a single abundance.

3.5 HCN abundance

In Figure 8 we present the range of HCN abundances across our parameter space. Unlike in the previous figures in this section, we have replaced the O/H ratio on the x-axis with the N/H ratio, with three values for the O/H ratio chosen to examine. As expected, HCN is strongly dependent on both the C/H and N/H ratios at the temperatures we model. While some dependence on the O/H ratio is also observed, this is merely a consequence of the O/H ratio affecting the overall C/O ratio.

We see a rapid increase in the abundance of HCN in the atmosphere for C/O ratios greater than 1. This is because the most abundant carbon carrier, CO, is no longer limited by the available carbon in the atmosphere, but by the available oxygen at these ratios. Thus, additional HCN can form due to the excess carbon

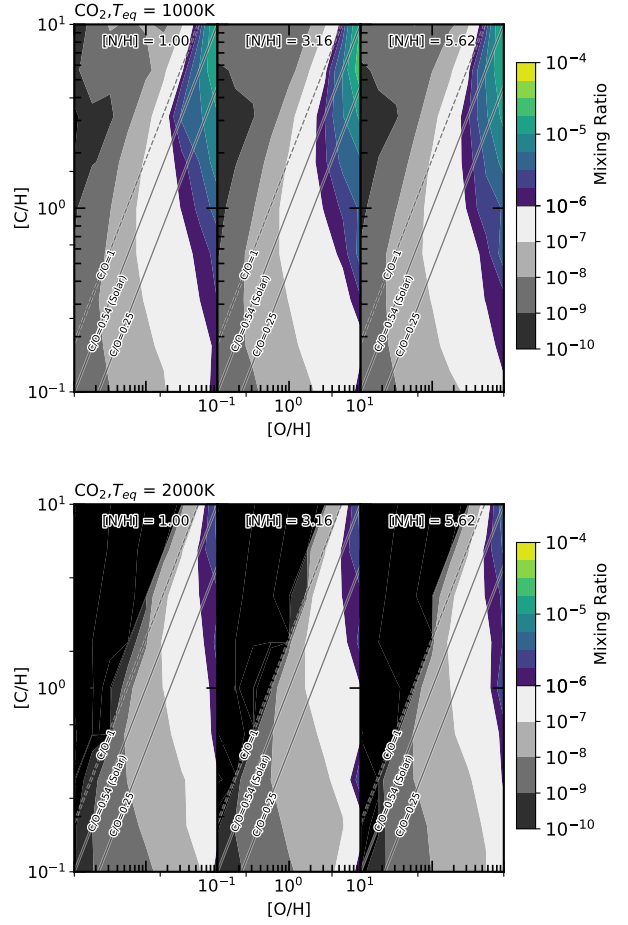


Figure 7. The abundance of CO_2 for two hot Jupiters, one with a 1000 K equilibrium temperature (top) and one with a 2000 K equilibrium temperature (bottom). The variation in abundance of CO_2 is shown against the atmospheric C/H and O/H ratios normalised to solar values. The C/O ratios of 0.25, 0.54 (solar) and 1 are shown on each plot to assist visualisation. Additionally, we consider three atmospheric N/H ratios normalised to solar; 1, 3.2 and 5.6. These are shown from left to right on the figures above.

available. Both planetary temperatures modelled have similar maximum abundances for HCN, at around 10^{-4} , at 10 [N/H] and $\text{C/O} \gg 1$. For C/O less than 1, we find that for lower temperatures we expect HCN abundances around 10^{-7} . For the hotter temperatures the HCN abundance is much lower, around 10^{-11} . The HCN abundance can function as a way of tracing the N/H ratio, however, for $\text{C/O} < 1$, highly sensitive measurements will be needed to detect HCN's predicted low abundances.

3.6 NH_3 abundance

In Figure 9 we present how the NH_3 abundance varies across our parameter space. As expected, NH_3 is dependent on the N/H ratio. We find that NH_3 is also dependent on the C/H and O/H ratio to a small extent, however this is mainly a function of the global C/O ratio, not the individual ratios themselves. Where the C/O ratio is greater than 1, we see large abundances of HCN, limiting the amount of available N to form NH_3 . We also see large differences in ammonia abundance between the two temperature models. At lower temperatures, with $\text{C/O} < 1$, the ammonia abundance varies

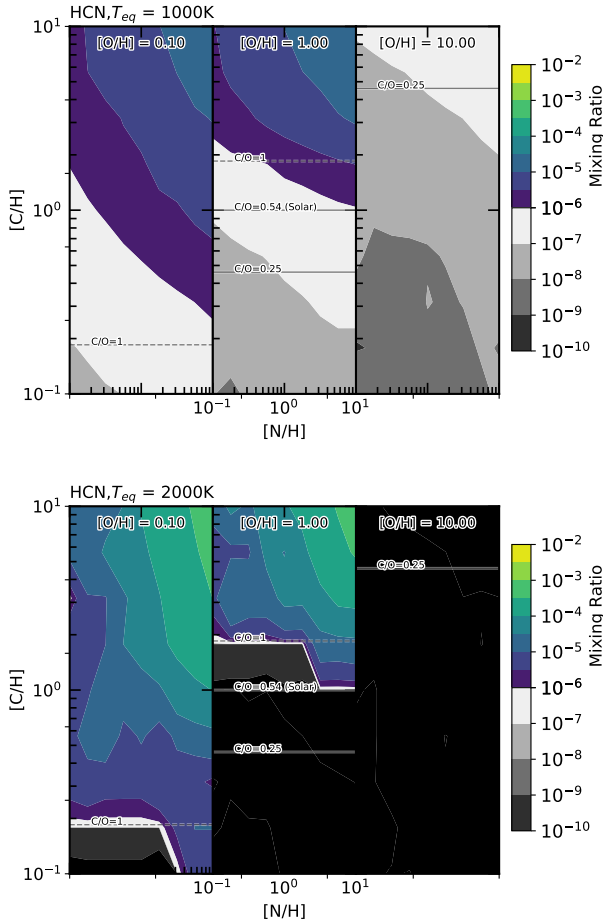


Figure 8. The abundance of HCN for two hot Jupiters, one with a 1000 K equilibrium temperature (top) and one with a 2000 K equilibrium temperature (bottom). The variation in abundance of HCN is shown against the atmospheric C/H and N/H ratios normalised to solar values. The C/O ratios of 0.25, 0.54 (solar) and 1 are shown on each plot to assist visualisation. Additionally, we consider three atmospheric O/H ratios normalised to solar; 0.1, 1 and 10. These are shown from left to right on the figures above.

between 10^{-5} and 10^{-4} . While in our higher temperature model we find approximately five orders of magnitude less ammonia in the atmosphere, between 10^{-10} and 10^{-9} for $C/O < 1$. The abundance of NH_3 is a useful tool to determine the N/H ratio for cooler planets, as long as sufficiently sensitive measurements to detect it in the atmosphere can be made.

4 COMPARISON WITH FORMATION AND MIGRATION MODELS

In this section we use our results from the previous section in conjunction with the formation models of [Madhusudhan et al. \(2014b\)](#); [Booth et al. \(2017\)](#); [Turrini et al. \(2021\)](#). We compare the metallicity ranges these works predict for different formation and migration models to the parameter figures in the previous section. This gives us a abundance range, for each of the six molecules investigated previously, for each formation and migration model. Thus, we can define what our model predicts the atmospheric composition of a hot Jupiter will be based upon where the planet formed and how it migrated.

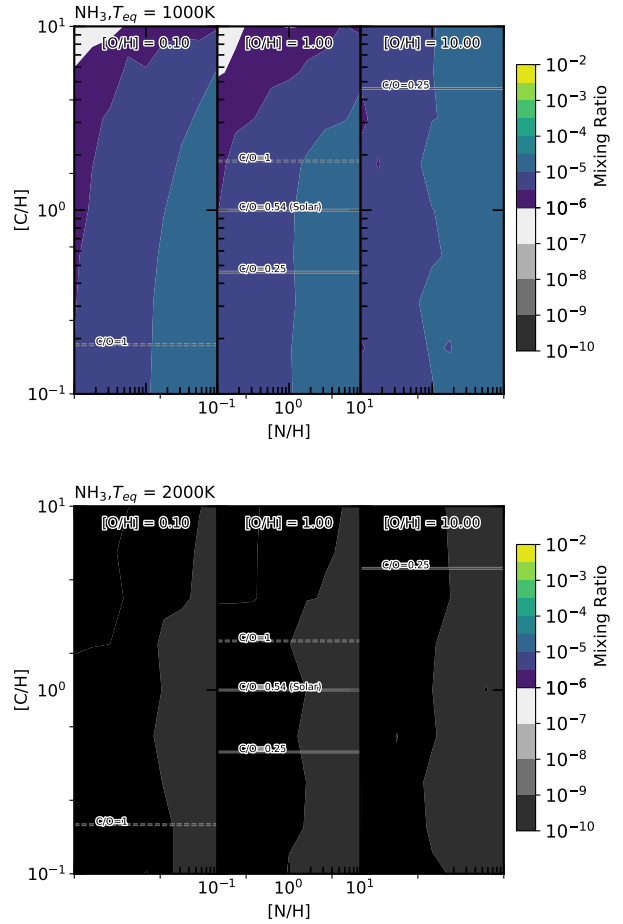


Figure 9. The abundance of NH_3 for two hot Jupiters, one with a 1000 K equilibrium temperature (top) and one with a 2000 K equilibrium temperature (bottom). The variation in abundance of NH_3 is shown against the atmospheric C/H and N/H ratios normalised to solar values. The C/O ratios of 0.25, 0.54 (solar) and 1 are shown on each plot to assist visualisation. Additionally, we consider three atmospheric O/H ratios normalised to solar; 0.1, 1 and 10. These are shown from left to right on the figures above.

4.1 Planetary Carbon and Oxygen abundances due to migration

From the work of [Madhusudhan et al. \(2014b\)](#), for a hot Jupiter formed via core accretion with subsequent disk migration to its current location, we expect $[C/H]$ ratios between 1 and 5, and $[O/H]$ ratios between 1 and 10, and that the C/O ratio is always less than solar. In Table 2 we show the range of expected chemical abundances of the six molecules we investigated in the previous section for this elemental parameter space.

We split planets formed by core accretion that then underwent disk-free migration into two groups: Those that formed beyond the CO_2 snowline, with sub-solar C/H and O/H and those that formed within the CO_2 snowline, with super-solar C/H and O/H . From [Madhusudhan et al. \(2014b\)](#), planets that formed within the CO_2 snowline, have allowed metallicities along the straight line between $[C/H]$ and $[O/H]$ equal to 1, and $[C/H] = 2$ and $[O/H] = 4$, and planets that formed beyond the CO_2 snowline have allowed metallicities along the straight line between $[C/H]$ and $[O/H]$ equal to 1, and $[C/H] = 0.6$ and $[O/H] = 0.4$. [Madhusudhan et al. \(2014b\)](#) did not consider the N/H in their models, and so we choose to use $N/H =$

Table 2. Expected abundance ranges for hot Jupiters formed by core accretion that migrate within the disk

Molecule	$\log(X_{\text{Max}}, X_{\text{Min}})$, 1000 K	$\log(X_{\text{Max}}, X_{\text{Min}})$, 2000 K
H ₂ O	(-2, -3.3)	(-2, -4)
CO	(-2.2, -3.2)	(-2, -3.3)
CH ₄	(-5, -6)	(-13, -14)
CO ₂	(-4, -7)	(-5, -7)
HCN	(-7, -8)	(-10, -12)
NH ₃	(-4.3, -5.3)	(-9.3, -10.3)

The expected mixing ratios for six molecules in the atmospheres of two hot Jupiters, one with $T_{\text{eq}} = 1000$ K and the other with $T_{\text{eq}} = 2000$ K, for a gas giant formed by core accretion that migrated within the disk, or a gas giant formed by gravitational instability between the CO₂ and CO snowline that migrated disk-free, from the work of [Madhusudhan et al. \(2014b\)](#).

Table 3. Expected abundance ranges for hot Jupiters formed by core accretion that migrate disk-free

Molecule	1000 K	2000 K
Within the CO ₂ snowline	$\log(X_{\text{Max}}, X_{\text{Min}})$	$\log(X_{\text{Max}}, X_{\text{Min}})$
H ₂ O	(-2.3, -3.3)	(-2, -4)
CO	(-3, -3.2)	(-2, -3.3)
CH ₄	(-4, -6)	(-13, -15)
CO ₂	(-5, -7)	(-6, -8)
HCN	(-7, -8)	(-11, -12)
NH ₃	(-4.3, -5.3)	(-9.3, -10.3)
Beyond the CO ₂ snowline		
H ₂ O	(-3, -4)	(-3, -5)
CO	(-3.3, -3.5)	(-3, -3.3)
CH ₄	(-4, -5)	(-8, -11)
CO ₂	(-6, -8)	(-7, -9)
HCN	(-6, -7)	(-9, -11)
NH ₃	(-4.3, -5.3)	(-9.3, -10.3)

The expected mixing ratios for six molecules in the atmospheres of two hot Jupiters, one with $T_{\text{eq}} = 1000$ K and the other with $T_{\text{eq}} = 2000$ K, for a gas giant formed by core accretion that underwent disk-free migration, from the work of [Madhusudhan et al. \(2014b\)](#). We split the formation location of the planet into two groups: Within the CO₂ snowline and beyond the CO₂ snowline.

1 for the comparisons here. We present the expected abundance for these planets in Table 3.

Lastly from the work of [Madhusudhan et al. \(2014b\)](#), we consider planets formed via gravitational instability that then migrate inwards disk-free. There are again two regions to consider for this formation-migration mechanism: Those planets that formed within the CO snowline and those that formed outside the CO snowline. The composition of those planets that formed by gravitational instability within the CO snowline is similar to those formed by core accretion with in-disk migration, however the potential metallicity also extends into sub-solar metallicity with super-solar C/O ratio. Those that formed beyond the CO snowline have a near solar C/O ratio, but with any metallicity within our parameter space, producing a wide range of possible abundances. We present the expected abundance ranges for both of these cases in Table 4.

We summarise the resulting atmospheric chemistry at 10^{-3} bar for our 1000 K and 2000 K hot Jupiters following formation and migration from these five different scenarios in Figure 10. Overall what we see is significant overlap between formation location and migration types investigated here. This was expected based upon the overlapping metallicities that we drew from [Madhusudhan et al. \(2014b\)](#). We can still draw some important insights from this data though.

H₂O: We find that high H₂O abundances in our models, be-

Table 4. Expected abundance ranges for hot Jupiters formed by gravitational instability that migrate disk-free

Molecule	1000 K	2000 K
Within the CO snowline	$\log(X_{\text{Max}}, X_{\text{Min}})$	$\log(X_{\text{Max}}, X_{\text{Min}})$
H ₂ O	(-2, -4)	(-2, -4)
CO	(-2.2, -3.5)	(-2, -4)
CH ₄	(-3.3, -6)	(-8.5, -14)
CO ₂	(-4, -7.5)	(-5, -10)
HCN	(-6, -8)	(-6, -12)
NH ₃	(-4.3, -5.3)	(-9.3, -10.3)
Beyond the CO snowline		
H ₂ O	(-2, -5)	(-2, -5)
CO	(-2.5, -5)	(-2, -4.5)
CH ₄	(-4, -5)	(-12, -13)
CO ₂	(-4, -9)	(-5, -10)
HCN	(-6.3, -7)	(-10, -11)
NH ₃	(-4.3, -5.3)	(-9.3, -10.3)

The expected mixing ratios for six molecules in the atmospheres of two hot Jupiters, one with $T_{\text{eq}} = 1000$ K and the other with $T_{\text{eq}} = 2000$ K, for a gas giant formed by gravitational instability and underwent disk-free migration from the work of [Madhusudhan et al. \(2014b\)](#). We split this formation mechanism for those planets formed outside of the CO snowline and those that formed within the CO snowline but beyond the CO₂ snowline.

tween 10^{-2} and 10^{-3} , can be found for a hot Jupiter that formed at any location, and is independent of the equilibrium temperature of the hot Jupiter. However, very low H₂O abundances were unique to planets that had formed further out, at least beyond the CO₂ snowline for both core accretion and gravitational instability formation models. This is because these formation locations resulted in either low O/H ratio or a high C/O ratio, both of which cause low H₂O abundances.

CO: Similar to H₂O, our model predicts high CO abundances in both cases are able to occur regardless of where the hot Jupiter formed. However, we once again find that very low CO abundances are only expected for planets that formed further out, either by core accretion beyond the CO₂ snowline or by gravitational instability beyond the CO snowline for our 1000K model, or any location of gravitational instability for our 2000K model. This is due to low C/H and O/H ratios, irrespective of the C/O ratio.

CH₄: For our 2000K temperature hot Jupiter, we never expect CH₄ to be detectable, with abundances always far below 10^{-6} . For our cooler 1000K hot Jupiter, methane abundances can be high, up to 10^{-4} for planets formed by core accretion with disk-free migration or gravitational instability beyond the CO snowline. We expect to see the highest CH₄ levels in the case of the 1000K hot Jupiter that formed between the CO₂ and CO snowlines, possibly approaching an abundance of 10^{-3} . This is because this is the model with the highest C/O ratio, on which the CH₄ ratio strongly depends. For our 1000K hot Jupiter, we only find methane abundances below 10^{-5} for planets that formed close in by core accretion, either within the CO₂ snowline and then migrated disk-free or those that underwent in-disk migration, or formed within the CO snowline by gravitational instability. It is possible then that detections of low levels of CH₄ could also function in helping determine where a hot Jupiter formed.

CO₂: For core accretion, our models find higher levels of CO₂ are associated with a planet that formed further in, with both the maximum and minimum levels of CO₂ increasing by up to two orders of magnitude as we move from the more distant formation models to the closer ones. However, planets that formed by gravitational instability, can contain a range of CO₂ levels that encompasses the entire range of all the other models, requiring other features to break the degeneracy here.

Table 5. Expected abundance ranges for hot Jupiters that became chemically enriched via pebble-drift

Molecule	1000 K	2000 K
Within the CO ₂ snowline	$\log(X_{\text{Max}}, X_{\text{Min}})$	$\log(X_{\text{Max}}, X_{\text{Min}})$
H ₂ O	(-3, -4.3)	(-3, -4)
CO	(-2.5, -3.2)	(-2.3, -3.3)
CH ₄	(-4, -5)	(-12, -13)
CO ₂	(-6, -7)	(-6, -7)
HCN	(-5, -7)	(-9, -10)
NH ₃	(-4.3, -5.3)	(-9.3, -10.3)
Beyond the CO ₂ snowline		
H ₂ O	(-3, -4.3)	(-3, -5)
CO	(-2, -5)	(-2, -4.3)
CH ₄	(-3, -4)	(-7, -9)
CO ₂	(-5, -9)	(-6, -9)
HCN	(-5, -7)	(-4, -7)
NH ₃	(-4.3, -5.3)	(-9.3, -10.3)

The expected mixing ratios for six molecules in the atmospheres of two hot Jupiters, one with $T_{\text{eq}} = 1000$ K and the other with $T_{\text{eq}} = 2000$ K, using the models of chemical enrichment by Booth et al. (2017). We split the formation location of the planet into two groups: Within the CO₂ snowline and beyond the CO₂ snowline.

HCN: For our 2000K temperature hot Jupiter, we predict HCN abundances below 10^{-8} , and thus very unlikely to be detectable, for every model except one: We find that our 2000K hot Jupiter formed by gravitational instability between the CO₂ and CO snowlines can have HCN abundances as high as 10^{-6} . In the atmosphere of our 1000K hot Jupiter, we only find high levels of HCN in the model of core accretion and then disk-free migration for planets that formed beyond the CO₂ snowline and gravitational instability within the CO snowline. This is because these are the only models with a significantly super-solar C/O ratio, which favours the production of HCN.

NH₃: Ammonia levels cover the same range in every model, with no expected metallicity to be extreme enough to find significantly different NH₃ levels. However, for our 2000K temperature hot Jupiter, the abundance of NH₃ in their atmospheres is expected to be below 10^{-8} , and thus not detectable. For the 1000K hot Jupiter, NH₃ is expected to be detectable at around 10^{-5} bar.

4.2 Chemical Enrichment of hot Jupiters

The work of Booth et al. (2017) looks at the chemical enrichment by pebble drift of gas giants formed by core accretion. For planets formed within the CO₂ snowline this results in $2 < [\text{C}/\text{H}] < 3$ and $[\text{O}/\text{H}] = 2$ and for planets formed beyond the CO₂ snowline this can result in any metallicity within our parameter space, but with a C/O = 1. The abundances our model predicts for this formation and migration scenario are in Table 5. We summarise the resulting atmospheric chemistry in 1000 K and 2000 K hot Jupiters following formation and migration from these two different scenarios in Figure 10.

Overall what we see is that only CH₄ and HCN in chemically enriched planets' atmospheres can stand out as tracers of these planets' pasts. Regardless of temperature, H₂O, CO, CO₂ and NH₃ all lie within the ranges of expected abundances discussed in the previous section. For only the 2000K hot Jupiters, do we find that chemical enrichment of planets formed beyond the CO₂ snowline leads to large elevations in the expected abundance of HCN. Also, our predicted CH₄ abundance in planets that have been chemically enriched by pebble drift having formed beyond the CO₂ snowline,

Table 6. Expected abundances for a hot Jupiters that formed at different locations within the disk

Molecule	5AU	12AU	19AU	50AU	100AU	130AU
1000 K	$\log(X)$	$\log(X)$	$\log(X)$	$\log(X)$	$\log(X)$	$\log(X)$
H ₂ O	-3.3	-3.2	-3.1	-3.0	-2.7	-2.5
CO	-3.4	-3.2	-3.1	-2.7	-2.7	-2.5
CH ₄	-4.4	-4.5	-4.2	-4.7	-5	-5.1
CO ₂	-6.7	-6.5	-6.1	-5.5	-5.2	-5.0
HCN	-6.5	-6.2	-6.3	-6.3	-6.1	-6.0
NH ₃	-5.1	-5.1	-5.0	-5.0	-4.7	-4.7
2000 K						
H ₂ O	-3.3	-3.3	-3.0	-2.3	-2.3	-2.3
CO	-3.3	-3.3	-3.0	-3.0	-2.5	-2.3
CH ₄	-12	-12	-12	-12	-12	-12
CO ₂	-7.3	-7.0	-7.0	-6.3	-6.0	-5.3
HCN	-10.3	-10.3	-10.3	-10.2	-10.1	-10
NH ₃	-10.2	-10.1	-10	-10	-9.7	-9.5

The expected mixing ratios for six molecules in the atmospheres of two hot Jupiters, one with $T_{\text{eq}} = 1000$ K and the other with $T_{\text{eq}} = 2000$ K, using the models Turrini et al. (2021). We split the table into columns of formation location of the planet, using the metallicity of these planets shown in Table 1 in conjunction with our models to produce the abundances shown in this table.

are at least half an order of magnitude above values expected by other formation models, making it the best contender for a chemical enrichment tracer.

There are a number of tracers to distinguish where a planet that was known to have been chemically enriched was formed. Both H₂O and CO abundances in enriched planets that formed beyond the CO₂ snowline are expected to be able to reach significantly lower values than in a planet formed within the CO₂ snowline. In hotter hot Jupiters, HCN can help distinguish two formation areas, however in cooler hot Jupiters there is a full overlap in the expected abundances of HCN from both locations. CH₄ likely works as the best tracer however. Regardless of temperature, there is no overlap in expected abundance of CH₄ between the two formation areas, with significantly higher CH₄ always being expected for a planet that formed beyond the CO₂ snowline.

4.3 Tracers of nitrogen chemistry

Turrini et al. (2021) select six formation locations in conjunction with a core accretion and in-disk model to produce the final metallicity of a hot Jupiter. These values are shown in Table 1. We tabulate the molecular abundance our model predicts for each planetary formation location in Table 6.

As expected, the monotonic increase in the metallicity of hot Jupiters as formation distance increases, translates to a similar monotonic increase for each of the six molecules we examine. This is shown in Figure 11. Notably, the molecules H₂O, CO, CH₄ and CO₂ all change by approximately an order of magnitude across the range of formation locations. This should be sufficient for detections of these molecules in a planet's atmosphere to link quite accurately to the planet's C/O ratio and where it formed. However, HCN and NH₃ have a significantly smaller range of possible abundances. This makes it much harder to be able to link the detection of nitrogen species to the planet's N/H ratio and where it may have formed, especially due to the current scarcity in nitrogen species detected and HCN being below the detectable limit regardless of planetary temperature.

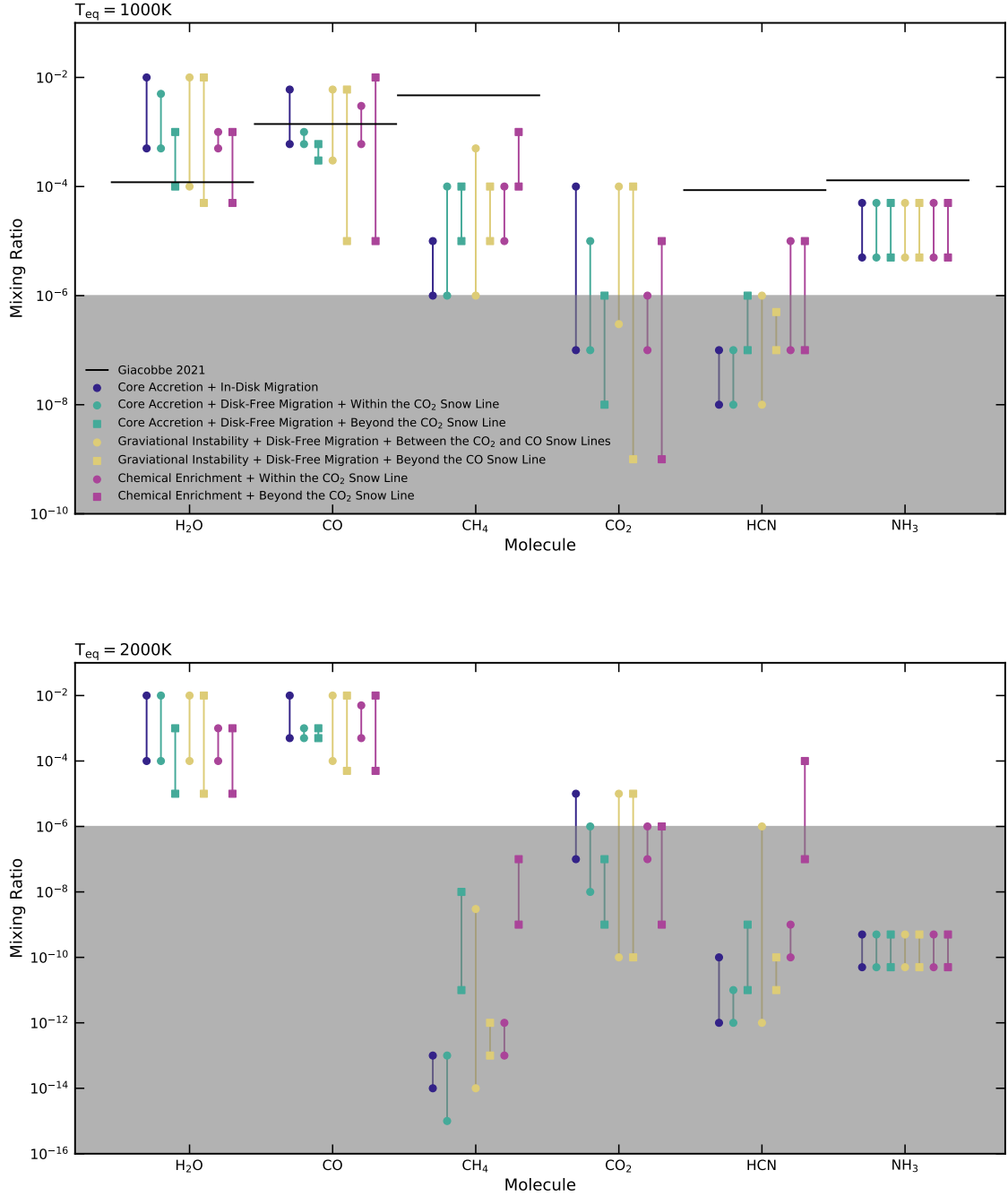


Figure 10. A comparison of the abundances of six molecules that our models predict, based upon the metallicities resulting from the five different formation and migration mechanisms discussed in Madhusudhan et al. (2014b) and two different formation locations from Booth et al. (2017), for the two different planet temperatures we investigate. The red, blue and green ranges correspond to work from Madhusudhan et al. (2014b) while the purple ranges correspond to work from Booth et al. (2017). The range of abundances we see for each species for each formation model is due to the spread of metallicity possible from those models. The grey zone below 10^{-6} marks the region in which abundances are expected to be too low to be detectable. The black horizontal lines indicated representative abundances for key molecules detected in (Giacobbe et al. 2021).

5 A COMPARISON WITH RETRIEVED ABUNDANCES IN HOT JUPITERS' ATMOSPHERES

In this section we examine an ensemble of molecular abundances measured in the atmospheres of hot Jupiters and compare them

to our model predictions. We also perform a case study on the hot Jupiter HD 209458b to investigate whether our models can constrain where the planet formed and how it migrated.

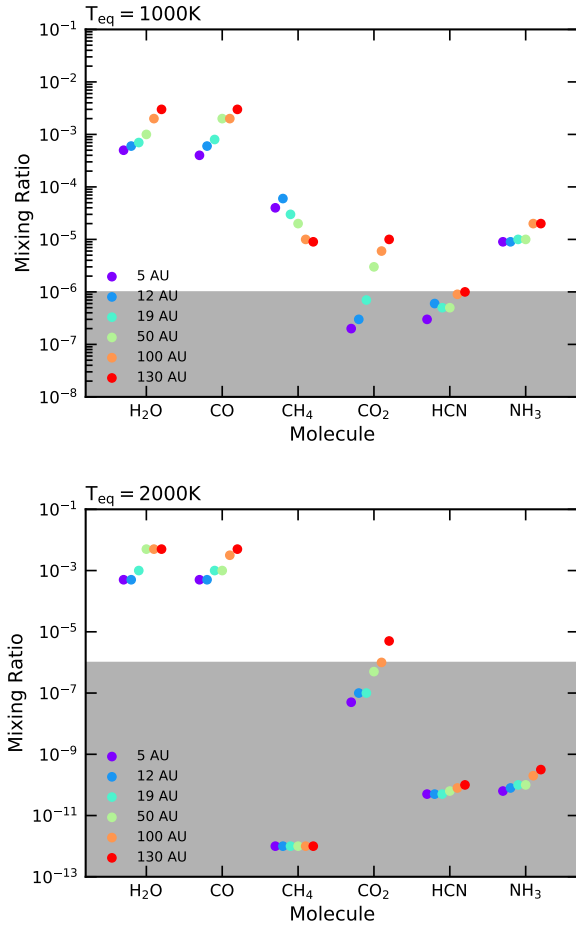


Figure 11. A comparison of the abundances of six molecules that our models predict for the different formation locations presented in Turrini et al. (2021), for hot Jupiters at two equilibrium temperatures. The grey zone below 10^{-6} marks the region in which abundances are expected to be too low to be detectable. The black lines for $T_{eq} = 1000\text{K}$ correspond to the values taken from Giacobbe et al. (2021), for comparisons made in Section 5

Planet Name	M_p (M_J)	T_{eq} (K)	$\log(X_{H_2O})$
WASP-107b	0.12	740	$-2.87^{+0.95}_{-0.73}$
HD 189733b	1.14	1200	$-4.66^{+0.35}_{-0.33}$
KELT-11b	0.20	1300	$-3.60^{+0.60}_{-0.70}$
HAT-P-1b	0.53	1320	$-2.54^{+0.75}_{-0.67}$
WASP-43b	2.03	1440	$-3.68^{+0.92}_{-0.88}$
HD 209458b	0.69	1450	$-4.54^{+0.33}_{-0.27}$
WASP-17b	0.51	1740	$-3.84^{+1.27}_{-0.51}$
WASP-19b	1.14	2050	$-3.43^{+0.47}_{-0.52}$

Table 7. A table of the H_2O abundances detected in hot Jupiters with equilibrium temperatures between 1000 K and 2000 K. The values for KELT-11b come from Changeat et al. (2020), while all the others were drawn from Welbanks et al. (2019).

5.1 H_2O abundances

H_2O is one of the most measured molecule in hot Jupiter atmospheres (e.g. Madhusudhan et al. 2014b; Kreidberg et al. 2014; Barstow et al. 2017; Pinhas et al. 2019; Welbanks et al. 2019). In Table 7 we show 8 hot Jupiters whose H_2O abundances have been determined to within an order of magnitude. All eight planets have their H_2O abundance fall within the ranges predicted by our models. However, HD 189773b and HD 209458b have notably lower H_2O abundances than any of the other planets. While the other planets could have formed and migrated by any of the mechanisms discussed in the previous section, our models suggest that HD 189733b and HD 209458b would have had to have formed further out to obtain their current water abundances. Which mechanism is still not precisely determined, but either core accretion, with or without chemical enrichment, beyond the CO_2 snowline, or gravitational instability beyond the CO snowline are the only ways to produce such low water mixing ratios within our models.

5.2 Case study HD 209458b

HD 209458b is one of the most studied hot Jupiters, with multiple molecules potentially detected within its atmosphere. Here we use the most recent abundance estimates for this planet. In particular, H_2O , CO and the C/O ratio on the day-side of the planet have been retrieved by Gandhi et al. (2019), and at the day-night terminator we can find values for the H_2O abundance in Welbanks et al. (2019) and the H_2O , CO, CH_4 , HCN and NH_3 abundance from Giacobbe et al. (2021). These values are summarised in Table 8. Based upon General Circulation Models (GCM) of HD 209458b (Showman et al. 2009), we can use our 2000 K model as an approximation to the day-side of the planet, and our 1000 K model as an approximation to the terminator of the planet. Comparing the retrieved values from the day-side emission spectra in Gandhi et al. (2019) to our results, we see that the detected values for H_2O and CO fall within the range of any of the formation models we considered. However, their retrieved C/O ratio of approximately 1 was only possible in one of the scenarios we investigated: Chemical enrichment via pebble drift, as discussed in Booth et al. (2017).

Next we compare our results to the retrieved abundances from the terminator transmission spectra of HD 209458b in Giacobbe et al. (2021). Both the H_2O and CO results are on the boundary of being possible with any formation model, but they do favour core accretion and chemical enrichment beyond the CO_2 snowline or any formation location by gravitational instability. All of the other abundances of retrieved molecules from Giacobbe et al. (2021) are higher than any our models predict. However, this difference is generally no more than half an order of magnitude, and so we will compare to the formation pathways that produce results closest to the retrieved values. It is likely that these differences arise from either margins of error within the retrieved values, or simplifications within our own models when trying to model the complex chemistry of hot Jupiters. The retrieved value for methane in Giacobbe et al. (2021) is approximately half an order of magnitude above our values of CH_4 for chemical enrichment beyond the CO_2 snowline and gravitational instability between the CO_2 and CO snowlines. However, it is several orders of higher than any other formation pathway, thus suggesting that for CH_4 , HD 209458b was likely to form via chemical enrichment beyond the CO_2 snowline or gravitational instability between the CO_2 and CO snowlines. The retrieved HCN abundance lies above any of our models predictions, but is within half an order of magnitude of values predicted by core accretion

Molecule	Emission (Gandhi et al. 2019)	Transmission (Welbanks et al. 2019)	Transmission (Giacobbe et al. 2021)	Matching Formation Models
H ₂ O	$-4.11^{+0.91}_{-0.3}$	$-4.54^{+0.33}_{-0.27}$	-3.92	All
CO	$-2.16^{+0.99}_{-0.47}$		-2.85	All
CH ₄			-2.33	~ CE-B or ~ GI-B
HCN			-4.07	~ CA-DF-B or ~ CE or ~ GI-B
NH ₃			-3.89	~ All
C/O ratio	$0.99^{+0.01}_{-0.02}$			CE or GI-B

Table 8. A summary of the retrieved values of molecular abundances in the atmosphere of HD 209458b from a number of recent studies. The matching formation models column refers to the formation models we compared to in Section 4. The abbreviations are: CE: Chemical Enrichment. CE-B: Chemical Enrichment beyond the CO₂ snowline. These models came from Booth et al. (2017). CA-ID: Core Accretion with In Disk migration. CA-DF-B: Core Accretion with Disk-Free Migration from beyond the CO₂ snowline. GI: Gravitational Instability. GI-B: Gravitational Instability between the CO₂ and CO snowlines. These models came from Madhusudhan et al. (2014b).

and disk-free migration beyond the CO₂ snowline, any location of chemical enrichment, or gravitational instability between the CO₂ and CO snowlines. Lastly, the NH₃ results from Giacobbe et al. (2021) are also higher than any of our modelled results, however this could be accounted for by variations in the N/H ratio. Regardless, any formation model could be responsible for producing the observed NH₃ values.

Overall, the likely formation location and migration mechanism for HD 209458b seems to be narrowed down significantly. The most likely pathway is forming between the CO₂ and CO snowlines by gravitational instability, since this fits with every detected feature. However, it is also possible that HD 209458b formed beyond the CO₂ snowline and was then chemically enriched by pebble accretion.

6 SUMMARY AND DISCUSSION

In this work we have explored the carbon, oxygen and nitrogen compositional parameter space for hot Jupiters, and seen how these predicted abundances may relate to their formation location. By expanding upon our previous work in Hobbs et al. (2019) we have run a suite of 1500 models of our chemical kinetics code. We did this for a generic hot Jupiter orbiting at two possible distances from a sun-like star, encompassing a range of atmospheric elemental compositions between 0.1x and 10x the solar values for carbon, oxygen and nitrogen. We compare our parameter space to the formation and migration models of three previous works (Madhusudhan et al. 2014b; Booth et al. 2017; Turrini et al. 2021) to create a framework of how the abundance of six of the major species in a hot Jupiter atmosphere might be linked to where the planet formed.

We find that, as expected, there is a large degree of degeneracy when trying to link a planet’s atmospheric composition to its formation location, however we do obtain some insights that may assist in narrowing down the history of a hot Jupiter. Using the relationship between formation and metallicity shown in Madhusudhan et al. (2014b) we find that low CO₂ and H₂O abundances can be expected only in planets forming beyond the CO₂ snowline. We also find that low CH₄ abundances on the cooler hot Jupiters are only expected for a planet forming within the CO₂ snowline or by gravitational instability beyond the CO₂ snowline. Additionally, we find that our models predict high HCN abundance for planets that formed beyond the CO₂ snowline via core accretion or by gravitational instability

between the CO₂ and CO snowlines, before undergoing disk-free migration.

We also considered the possibility of chemical enrichment of hot Jupiters as presented in Booth et al. (2017). We find the best way to determine if a hot Jupiter had been chemically enriched was via an elevated CH₄ abundance within the enriched planet’s atmosphere. The formation location of a chemically enriched planet could best be identified via the CO or CO₂ abundance, both of which would be lower in a planet that formed beyond the CO₂ snowline.

Using the work of Turrini et al. (2021), we investigated whether having the N/H ratio as a chemical parameter could allow us to gain insights into where a hot Jupiter formed. In general we find that this is not the case. Species that do not contain nitrogen are generally unaffected by changes to the N/H ratio. Additionally, the range of N/H ratios predicted by Turrini et al. (2021) only covers between $1 < [N/H] < 3$, which does not have a very significant impact even on those species that do contain nitrogen.

We compared an ensemble of retrieved H₂O abundances on hot Jupiters from Welbanks et al. (2019) to the H₂O abundances we predicted using our models. We found that all the detected abundances lay within our predictions but, with only the H₂O abundance available, in most cases it was not possible to distinguish which specific formation mechanism may have lead to that abundance. However, in two cases (HD 189733b and HD 209458b) where the H₂O abundances are significantly sub-solar (Madhusudhan et al. 2014a; Barstow et al. 2017; Pinhas et al. 2019; Welbanks et al. 2019), our models suggest their formation beyond the CO₂ or CO snowlines followed by disk-free migration. Our results are consistent with previous studies which used such low H₂O abundances in hot Jupiters to suggest their formation beyond the snowlines and disk free migration (e.g. Madhusudhan et al. 2014b; Brewer et al. 2017; Welbanks et al. 2019).

Finally we performed a case study on the hot Jupiter HD 209458b, using multiple molecular detections from Gandhi et al. (2019), Welbanks et al. (2019) and Giacobbe et al. (2021). Our model predicted formation between the CO₂ and CO snowlines followed by disk free migration as the most likely origin for this planet. This inference assumed a formation model based on gravitational instability, from Madhusudhan et al. (2014b), but formation by core accretion at the same location may also be possible. Similarly, core accretion beyond the CO₂ snowline followed by chemical enrichment by pebble drift (Booth et al. 2017) also matched with all but one molecular detection, and thus could also be a contender for how HD 209458b was formed.

There are naturally some caveats to our results based upon the assumptions made within our modelling. The first of these is the common assumption that the metallicity of the protoplanetary disk is solar. Combining our model results with a planet that formed in an environment that had a significantly super or sub solar metallicity would not allow us to accurately trace a planet back to its formation mechanism and location. Additionally, our model used standardised stellar and planetary properties (i.e., The star was solar equivalent, and the planet modelled was always tidally locked and of a constant mass and radius). These values would be needed to run accurate models of a specific planet. Lastly, chemistry due to other elemental species, such as sulfur, has shown to be able to influence the abundances of the species that we have modelled in this work. Thus, the accuracy of these models could be improved by including these additional species.

To improve our ability to predict formation mechanisms further we need additional, more accurate, molecular abundance measurements on hot Jupiters, and to expand the functionality of our code to consider a wider range of planetary and stellar properties. The upcoming launch of satellites such as the James Web Space Telescope (JWST) should help in providing a more accurate picture of the composition of a hot Jupiter. To improve chemical models of hot Jupiters, inclusion of other elements such as sulfur may assist in making the models more accurate representations of their atmospheric chemistry and breaking degeneracies of formation location.

ACKNOWLEDGEMENTS

R.H. and O.S. acknowledge support from the UK Science and Technology Facilities Council (STFC).

DATA AVAILABILITY

The data underlying this article will be shared on reasonable request to the corresponding author.

REFERENCES

- Asplund M., Grevesse N., Sauval A. J., Scott P., 2009, *ARA&A*, **47**, 481
- Barstow J. K., Aigrain S., Irwin P. G. J., Sing D. K., 2017, *ApJ*, **834**, 50
- Boley A. C., 2009, *ApJ*, **695**, L53
- Boley A. C., Durisen R. H., 2010, *ApJ*, **724**, 618
- Booth R. A., Clarke C. J., Madhusudhan N., Ilee J. D., 2017, *MNRAS*, **469**, 3994
- Bosman A. D., Cridland A. J., Miguel Y., 2019, *A&A*, **632**, L11
- Boss A. P., 1997, *Science*, **276**, 1836
- Boss A. P., 2000, *ApJ*, **536**, L101
- Brewer J. M., Fischer D. A., Madhusudhan N., 2017, *AJ*, **153**, 83
- Changeat Q., Edwards B., Al-Refaie A. F., Morvan M., Tsiaras A., Waldmann I. P., Tinetti G., 2020, *AJ*, **160**, 260
- Cridland A. J., Pudritz R. E., Alessi M., 2016, *MNRAS*, **461**, 3274
- Cridland A. J., van Dishoeck E. F., Alessi M., Pudritz R. E., 2020, *A&A*, **642**, A229
- Eistrup C., Walsh C., van Dishoeck E. F., 2018, *A&A*, **613**, A14
- Forgan D., Rice K., 2011, *MNRAS*, **417**, 1928
- Gammie C. F., 2001, *ApJ*, **553**, 174
- Gandhi S., Madhusudhan N., Hawker G., Piette A., 2019, *AJ*, **158**, 228
- Giacobbe P., et al., 2021, *Nature*, **592**, 205
- Greene T. P., Line M. R., Montero C., Fortney J. J., Lustig-Yaeger J., Luther K., 2016, *ApJ*, **817**, 17
- Guillot T., 2010, *A&A*, **520**, A27
- Helled R., Bodenheimer P., 2010, *Icarus*, **207**, 503
- Helled R., et al., 2014, in Beuther H., Klessen R. S., Dullemond C. P., Henning T., eds, *Protostars and Planets VI*. p. 643 ([arXiv:1311.1142](https://arxiv.org/abs/1311.1142)), doi:10.2458/azu_uapress_9780816531240-ch028
- Helling C., Woitke P., Rimmer P. B., Kamp I., Thi W.-F., Meijerink R., 2014, *Life*, **4**, 142
- Hobbs R., Shorttle O., Madhusudhan N., Rimmer P., 2019, *MNRAS*, **487**, 2242
- Hobbs R., Rimmer P. B., Shorttle O., Madhusudhan N., 2021, *MNRAS*, **500**, 1
- Khorshid N., Min M., Désert J. M., Woitke P., Dominik C., 2021, *arXiv e-prints*, p. [arXiv:2111.00279](https://arxiv.org/abs/2111.00279)
- Kobayashi H., Tanaka H., Krivov A. V., 2011, *ApJ*, **738**, 35
- Komacek T. D., Showman A. P., Parmentier V., 2019, *ApJ*, **881**, 152
- Kreidberg L., et al., 2014, *ApJ*, **793**, L27
- Lissauer J. J., Stevenson D. J., 2007, in Reipurth B., Jewitt D., Keil K., eds, *Protostars and Planets V*. p. 591
- Madhusudhan N., 2012, *ApJ*, **758**, 36
- Madhusudhan N., 2019, *ARA&A*, **57**, 617
- Madhusudhan N., Crouzet N., McCullough P. R., Deming D., Hedges C., 2014a, *ApJ*, **791**, L9
- Madhusudhan N., Amin M. A., Kennedy G. M., 2014b, *ApJ*, **794**, L12
- Madhusudhan N., Agúndez M., Moses J. I., Hu Y., 2016, *Space Sci. Rev.*, **205**, 285
- Martín-Doménech R., Muñoz Caro G. M., Bueno J., Goesmann F., 2014, *A&A*, **564**, A8
- Mayor M., Queloz D., 1995, *Nature*, **378**, 355
- Mordasini C., van Boekel R., Mollière P., Henning T., Benneke B., 2016, *ApJ*, **832**, 41
- Moses J. I., et al., 2011, *ApJ*, **737**, 15
- Moses J. I., et al., 2013, *The Astrophysical Journal*, **777**, 34
- Öberg K. I., Wordsworth R., 2019, *AJ*, **158**, 194
- Öberg K. I., Murray-Clay R., Bergin E. A., 2011, *ApJ*, **743**, L16
- Papaloizou J. C. B., Nelson R. P., Kley W., Masset F. S., Artymowicz P., 2007, in Reipurth B., Jewitt D., Keil K., eds, *Protostars and Planets V*. p. 655 ([arXiv:astro-ph/0603196](https://arxiv.org/abs/astro-ph/0603196))
- Pinhas A., Madhusudhan N., Gandhi S., MacDonald R., 2019, *MNRAS*, **482**, 1485
- Pollack J. B., Hubickyj O., Bodenheimer P., Lissauer J. J., Podolak M., Greenzweig Y., 1996, *Icarus*, **124**, 62
- Pudritz R. E., Cridland A. J., Alessi M., 2018, *Connecting Planetary Composition with Formation*. p. 144, doi:10.1007/978-3-319-55333-7_144
- Showman A. P., Fortney J. J., Lian Y., Marley M. S., Freedman R. S., Knutson H. A., Charbonneau D., 2009, *ApJ*, **699**, 564
- Tsai S.-M., Lyons J. R., Grosheintz L., Rimmer P. B., Kitzmann D., Heng K., 2017, *ApJS*, **228**, 20
- Turrini D., et al., 2021, *ApJ*, **909**, 40
- Venot O., Hébrard E., Agúndez M., Dobrijevic M., Selsis F., Hersant F., Iro N., Bounaceur R., 2012, *A&A*, **546**, A43
- Venturini J., Alibert Y., Benz W., 2016, *A&A*, **596**, A90
- Welbanks L., Madhusudhan N., Allard N. F., Hubeny I., Spiegelman F., Leininger T., 2019, *ApJ*, **887**, L20
- Wu Y., Lithwick Y., 2011, *ApJ*, **735**, 109
- Wu Y., Murray N., 2003, *ApJ*, **589**, 605
- Zahnle K., Marley M. S., Morley C. V., Moses J. I., 2016, *ApJ*, **824**, 137
- Zhang X., Showman A. P., 2017, *ApJ*, **836**, 73

This paper has been typeset from a \LaTeX file prepared by the author.